EPSC Abstracts
Vol. 13, EPSC-DPS2019-566-1, 2019
EPSC-DPS Joint Meeting 2019

EPSC
EPSC-DPS Joint Meeting 2019
15–20 September 2019 | Geneva, Switzerland

Mini-RF S- and X-band Bistatic Observations of the Moon

G. Wesley Patterson (1), Lynn M. Carter (2), Angela M. Stickle (1), Joshua T. S. Cahill (1), Michael C. Nolan (2), Gareth A. Morgan (3), Dustin M. Schroeder (4), and the Mini-RF Team
(1) Johns Hopkins University Applied Physics Laboratory, Laurel, MD (Wes.Patterson@jhuapl.edu), (2) Lunar and Planetary Laboratory, Tucson AZ, (3) Planetary Science Institute, Tucson AZ, (4) Stanford University, Stanford CA.

Abstract

Mini-RF S- and X-band bistatic observations of the Moon are being acquired to address science objectives of the NASA Lunar Reconnaissance Orbiter (LRO). These data are providing, among other things, insight into the distribution of water ice at the lunar poles, how impacts are producing regolith on the Moon and other airless bodies, and how lunar volcanism has evolved over time.

1. Introduction

NASA's Mini-RF instrument on the Lunar Reconnaissance Orbiter (LRO) is currently operating in concert with the Arecibo Observatory (AO) and the Goldstone deep space communications complex 34 meter antenna DSS-13 to collect bistatic radar data of the Moon. These data provide a means to characterize the scattering properties of the upper meter(s) of the lunar surface, as a function of bistatic angle, at S-band (12.6 cm) and X-Band (4.2 cm) wavelengths. These data are being collected to address LRO science objectives related to: the vertical distribution of lunar water; the form and abundance of lunar water ice; how impacts expose and break down rocks to produce regolith on the Moon and other airless bodies; the present rate of regolith gardening; and how lunar volcanism has evolved over time.

2. Background

The transmitters for Mini-RF bistatic observations are AO (S-band) and DSS-13 (X-band). For each observation, the lunar surface is illuminated with a circularly polarized, chirped signal that tracks the Mini-RF antenna boresight intercept on the surface of the Moon. The Mini-RF receiver operates continuously and separately receives the horizontal and vertical polarization components of the signal backscattered from the lunar surface. The resolution of the data is ~100 m in range and ~2.5 m in azimuth but can vary from one observation to another, as a function of the viewing geometry. For analysis, the data are averaged in azimuth to provide a spatial resolution of 100 m. This yields an ~25-look average for each sampled location.

The data returned provide information on the structure (i.e., roughness) and dielectric properties of surface and buried materials within the penetration depth of the system (up to several meters for Mini-RF) [1-4]. The bistatic architecture allows examination of the scattering properties of a target surface for a variety of bistatic angles. Laboratory data and analog experiments, at optical wavelengths, have shown that the scattering properties of lunar materials can be sensitive to variations in bistatic angle [5-7].

3. Operations

Collecting data in the Mini-RF bistatic architecture requires significant advance planning with both the LRO operations team and ground-based facilities. As a result, no more than a few collects per month are feasible. The first Mini-RF bistatic campaign (2012-2015) included 28 AO S-band observations of the lunar surface – polar and nonpolar. Those observations provided data used to suggest the presence of water ice within floor materials of the crater Cabeus [8] and to characterize the weathering of Copernican crater ejecta [8,9].

The current bistatic campaign (2017-present) includes an additional 4 AO S-band observations and 35 DSS-13 X-band observations of the lunar surface (Figure 1). A variety of lunar terrains are being targeted to address science objectives for the ongoing LRO extended mission. They include collecting data of: the floors of south polar craters to search for signatures indicative of the presence of water ice [10]; Copernican crater ejecta blankets to characterize rates of regolith breakdown/weathering [11,12]; the ejecta

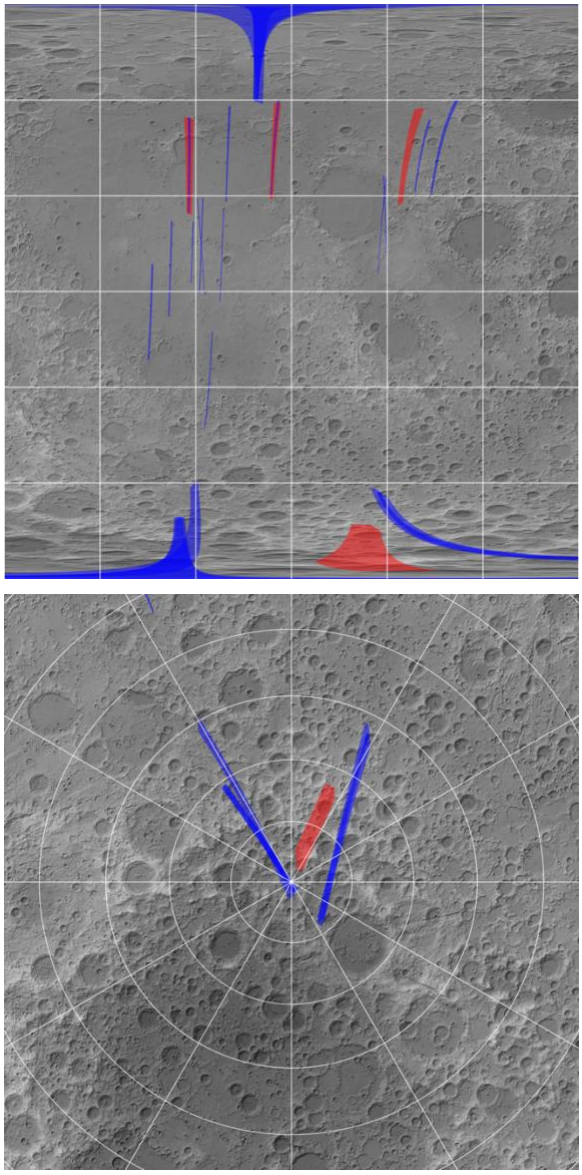

Figure 1: S-band (red) and X-band (blue) radar coverage in the second bistatic campaign for the lunar nearside (top; 90°W to 90°E) and south pole (bottom; 60°S to 90°S)

of newly-formed craters to characterize the size-distribution and density of wavelength-scale scatters as a function of distance from the impact [13]; mare materials within the Imbium basin to provide important information on the locations, extents, and depths flow units and deposits [14]; and irregular mare patches (IMPs) and pyroclastic deposits to characterize their radar properties [15,16]. In concert with the collection of these data, modeling work is being conducted to characterize the response of surface materials to variations in incidence angle [17] and to address LRO science objectives with Mini-RF monostatic data [e.g., 18,19].

4. Results

Initial analysis of south polar targets acquired at X-band [10] do not appear to show the potential water ice signature detected at S-band [8]. This would indicate that, if water ice is present in Cabeus crater floor materials, it is buried beneath ~0.5 m of regolith that does not include radar-detectible deposits of water ice. Observations of Copernican crater ejecta materials at S- and X-band wavelengths continue to show variations that can be attributed to the age of the crater [11]. Differences between S- and X-band observations of the same crater are also present, providing new insight into the size-distribution of radar scatters within the ejecta [11,12]. Two craters that formed during the LRO mission have been identified in X-band Mini-RF data acquired in the current bistatic campaign. Analysis of these data suggest enhanced wavelength-scale surface roughness to radial distances of 100s of meters from the crater centers [13]. S- and X-band observations of mare materials in the Imbrium basin and pyroclastic deposits in the Montes Carpatus, Aristarchus, and Taurus Littrow regions have been acquired and, combined with ground-based P-band observations, are providing important information on the locations, extents, and depths to individual flow units and deposits [14-16].

References

[1] Campbell et al. (2010), *Icarus*, 208, 565-573; [2] Raney et al. (2012), *JGR*, 117, E00H21; [3] Carter et al. (2012), *JGR*, 117, E00H09; [4] Campbell (2012), *JGR*, 117, E06008; [5] Hapke et al. (1998), *Icarus*, 133, 89-97; [6] Nelson et al. (2000), *Icarus*, 147, 545-558; [7] Piatek et al. (2004), *Icarus*, 171, 531-545. [8] Patterson et al. (2017), *Icarus*, 283, 2-19; [9] Stickle et al. (2016), *47th LPSC* #2928; [10] Patterson et al. (2018), *49thLPSC* #2007; [11] Stickle et al. (2018), *49thLPSC* #1585; [12] Novak et al. (2018), *49thLPSC* #2915; [13] Cahill et al. (2018), *49thLPSC* #2693; [14] Morgan et al. (2018), *49thLPSC* #1897; [15] Carter et al. (2018), *49thLPSC* #2461; [16] Sriram et al. (2018), *49thLPSC* #2496; [17] Prem et al. (2018), *49thLPSC* #2134; [18] Nypaver et al. (2018), *49thLPSC* #2560; [19] Mandt et al. (2018), *49thLPSC*.